

**Ovipositor-inspired steerable needle  
design and preliminary experimental evaluation**

Scali, Marta; Pusch, T.P.; Breedveld, Paul; Dodou, Dimitra

**DOI**

[10.1088/1748-3190/aa92b9](https://doi.org/10.1088/1748-3190/aa92b9)

**Publication date**

2018

**Document Version**

Final published version

**Published in**

Bioinspiration & Biomimetics: learning from nature

**Citation (APA)**

Scali, M., Pusch, T. P., Breedveld, P., & Dodou, D. (2018). Ovipositor-inspired steerable needle: design and preliminary experimental evaluation. *Bioinspiration & Biomimetics: learning from nature*, 13(1), Article 016006. <https://doi.org/10.1088/1748-3190/aa92b9>

**Important note**

To cite this publication, please use the final published version (if applicable).  
Please check the document version above.

**Copyright**

Other than for strictly personal use, it is not permitted to download, forward or distribute the text or part of it, without the consent of the author(s) and/or copyright holder(s), unless the work is under an open content license such as Creative Commons.

**Takedown policy**

Please contact us and provide details if you believe this document breaches copyrights.  
We will remove access to the work immediately and investigate your claim.

***Green Open Access added to TU Delft Institutional Repository***

***'You share, we take care!' – Taverne project***

**<https://www.openaccess.nl/en/you-share-we-take-care>**

Otherwise as indicated in the copyright section: the publisher is the copyright holder of this work and the author uses the Dutch legislation to make this work public.

PAPER

## Ovipositor-inspired steerable needle: design and preliminary experimental evaluation

To cite this article: M Scali *et al* 2018 *Bioinspir. Biomim.* **13** 016006

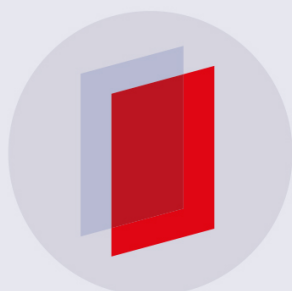
View the [article online](#) for updates and enhancements.

### Related content

- [Laser Doppler sensing for blood vessel detection with a biologically inspired steerable needle](#)  
V Virdyawan, M Oldfield and F Rodriguez y Baena
- [Novel design of honeybee-inspired needles for percutaneous procedure](#)  
Mohammad Sahlabadi and Parsaoran Hutapea
- [Buckling prevention strategies in nature as inspiration for improving percutaneous instruments: a review](#)  
Aimée Sakes, Dimitra Dodou and Paul Breedveld

### Recent citations

- [Experimental evaluation of a self-propelling bio-inspired needle in single- and multi-layered phantoms](#)  
M. Scali *et al*
- [How Does Biologically Inspired Design Cope with Multi-Functionality?](#)  
Nicklas Svendsen and Torben Anker Lenau



**IOP | ebooks™**

Bringing you innovative digital publishing with leading voices to create your essential collection of books in STEM research.

Start exploring the collection - download the first chapter of every title for free.

# Bioinspiration & Biomimetics



## PAPER

# Ovipositor-inspired steerable needle: design and preliminary experimental evaluation

RECEIVED  
14 August 2017

ACCEPTED FOR PUBLICATION  
11 October 2017

PUBLISHED  
5 December 2017

M Scali<sup>1,3</sup>, T P Pusch<sup>2,3</sup>, P Breedveld<sup>1</sup> and D Dodou<sup>1</sup>

<sup>1</sup> Faculty of Mechanical, Maritime and Materials Engineering, Biomechanical Department, Delft University of Technology, Delft, The Netherlands

<sup>2</sup> Fraunhofer Project Group for Automation in Medicine and Biotechnology, Fraunhofer Institute for Manufacturing Engineering and Automation, Mannheim, Germany

<sup>3</sup> Joint first authors.

E-mail: [m.scali@tudelft.nl](mailto:m.scali@tudelft.nl)

**Keywords:** medical needles, steerable needles, percutaneous procedures, biologically inspired, solid organs

Supplementary material for this article is available [online](#)

## Abstract

Flexible steerable needles have the potential to allow surgeons to reach deep targets inside the human body with higher accuracy than rigid needles do. Furthermore, by maneuvering around critical anatomical structures, steerable needles could limit the risk of tissue damage. However, the design of a thin needle (e.g. diameter under 2 mm) with a multi-direction steering mechanism is challenging. The goal of this paper is to outline the design and experimental evaluation of a biologically inspired needle with a diameter under 2 mm that advances through straight and curved trajectories in a soft substrate without being pushed, without buckling, and without the need of axial rotation. The needle design, inspired by the ovipositor of parasitoid wasps, consisted of seven nickel titanium wires and had a total diameter of 1.2 mm. The motion of the needle was tested in gelatin phantoms. Forward motion of the needle was evaluated based on the lag between the actual and the desired insertion depth of the needle. Steering was evaluated based on the radius of curvature of a circle fitted to the needle centerline and on the ratio of the needle deflection from the straight path to the insertion depth. The needle moved forward inside the gelatin with a lag of 0.21 (single wire actuation) and 0.34 (double wire actuation) and achieved a maximum curvature of  $0.0184\text{ cm}^{-1}$  and a deflection-to-insertion ratio of 0.0778. The proposed biologically inspired needle design is a relevant step towards the development of thin needles for percutaneous interventions.

## 1. Introduction

Medical needles are commonly used in percutaneous procedures, where accurate and precise tissue targeting is required to obtain diagnostic samples [1, 2], position radioactive seeds [3, 4], and deliver drugs [5, 6]. Needle placement can be affected by several factors, such as needle deflection due to needle-tissue interaction, organ movement due to physiological processes (e.g. breathing), and human error [7]. If the needle is misplaced, intraoperative adjustment of the needle path or reinsertion of the needle is necessary, which could increase the risk and extent of tissue damage and the intervention time.

While rigid needles allow for small adjustments around a straight path, flexible steerable needles can follow curved trajectories, which might improve accuracy and precision in reaching target tissues [8].

Moreover, flexible steerable needles are likely to limit the risk of tissue damage by maneuvering around critical anatomical structures (e.g. blood vessels) that are laid along the needle trajectory towards the target.

### 1.1. Steerable needle mechanism

Several steerable needle designs and mechanisms have been described in the literature (for a review, see [9]). Two main methods for steering can be distinguished: steering due to a pre-defined needle shape and due to a means of actuation.

Bevel-tip needles [10–13] and pre-curved needles [14, 15] are examples of needles with a pre-defined shape. When a bevel-tip needle is inserted into the tissue, off-axis reaction forces at the tip bend the needle in the direction of the bevel [16, 17]. The curvature of the needle is usually controlled by rotating the needle while it is advanced through the tissue [18]. Several

variations of bevel-tip needles have been proposed in order to increase the maximum curvature of the needle. For example, Swaney *et al* [10] presented a bevel-tip needle with a flexure joint that is thinner than the needle body, and Wang *et al* [12] added articulations along the body of a bevel-tip needle, with both modifications allowing for a larger deflection of the needle upon insertion in the tissue than a standard bevel-tip needle. Another way to increase the steering curvature is by increasing the diameter of the tip with respect to the diameter of the body which leads to a larger contact area with the tissue compared to a standard bevel-tip needle [13]. Also in pre-curved needles off-axis reaction forces are generated at the tip by the surrounded tissue, causing the needle to bend upon insertion into the tissue. Pre-curved needles commonly consist of a pre-curved stylet (internal tube) and a straight cannula (external tube) [14]. The needle follows a straight direction when the stylet is fed through the cannula and curves once the stylet is pushed forward. Notches of different shapes and dimensions have been added to the pre-curved stylet in order to increase the flexibility and hence the steering curvature [19]. Needle designs with both the stylet and the cannula pre-curved [20] or with a pre-curved stylet bearing a bevel-tip [21] are two other variations used to achieve a high curvature. Steering in multiple directions is achieved by rotating the needle shaft around its axis. Multiple pre-curved tubes can be also arranged in a telescopic way, creating a so-called ‘active cannula’ [22], where the final curvature is a result of the amount of rotation and extension provided by each of the tubes. A hybrid approach was presented by Bui *et al* [23], where the needle consists of a straight cannula and a straight stylet with a bevel-tip. In this case, the amount of steering is a function of the offset between the bevel-tip and the cannula.

An example of needles that steer due to a means of actuation are tendon-driven needles [24–26]. Tendon-driven needles use a mechanical actuation means (e.g. cables) to deflect the tip and draw a curved path. Van de Berg *et al* [24] presented a tendon-actuated flexible needle that steers by means of four cables running over a ball joint placed near the tip. Adebare *et al* [26] used Nitinol pull wires and a miniaturized cable pulley to actuate a flexural conical tip. Shape-memory or pseudoelastic materials have also been used as actuation means for needle steering [27, 28]. For example, Ayvali *et al* [27] described a needle made out of segments interconnected by shape memory alloy wires that deflect in response to Joule heating. Konh *et al* [28] used an SMA-wire to connect the body of the needle with a bevel-tip. The wire is used to control the deflection angle of the needle. In the design of Yan *et al* [29] the deflection of the needle is controlled by piezoelectric actuators. These are placed on the external surface of the needle, and by applying an electrical field a longitudinal strain is induced, resulting in deflection of the needle.

Despite the potential of flexible steerable needles, some functional limitations can also be identified. Needles with a predefined shape mostly steer in 2D with a constant radius, meaning that for steering in 3D with a variable radius, axial rotation of the needle is needed. Rotating a needle while it is being advanced through the tissue can generate a torsional stress on the needle body. This may in turn result in angular lag between the orientation of the needle base and the needle tip, making the control of the needle trajectory difficult [30, 31]. Actuated needles do allow for steering in 3D without axial rotation, but actuating elements requires space, inhibiting the miniaturization of this type of needles. Moreover, both in needles with predefined shape and actuated needles, buckling can occur when they are pushed deep into the tissue, which compromises their structural integrity and the safety of the medical procedure [32].

## 1.2. Biological inspiration for steerable needles

In nature, several species of parasitoid wasps possess a thin and flexible needle-like structure, called ovipositor, which is used to deposit eggs in a host (e.g. a larva) hidden into tree trunks (e.g. the wasp species *Megarhyssa atrata* [33]) or fruits (e.g. the wasp species *Apocrypta westwoodi* [34]) (figure 1(a)). The wasp ovipositor holds promise as a biological paradigm for medical needles, as it avoids buckling despite the fact that it is long and thin (with an aspect ratio higher than 200 in some species [35]) and is presumably able to steer in 3D without axial rotation.

The wasp ovipositor consists of three longitudinal segments called valves: two ventral valves and one dorsal valve. The valves are mechanically interlocked by means of a jigsaw-puzzle-like mechanism, called olistheter, but can still slide along each other, actuated by abdominal musculature (figure 1(c)) [36]. The wasp advances the ovipositor through the substrate by moving the valves antagonistically: one ventral valve is advanced forward at a time, while the other ventral valve and the dorsal valve are standing still or pulled backwards. Directional serrations at the ovipositor tip allow the stationary/pulled backwards valves to anchor against the substrate [37] (figure 1(b)). The created pretension in the ovipositor and friction against the substrate compensates for the dynamic friction force along the advancing valve and the forces at the tip of the valve, thereby preventing buckling of the ovipositor [35].

Next to buckling prevention and advancement of the ovipositor along a straight path, the wasp is presumably also able to steer the ovipositor along 3D-curved trajectories. Several hypotheses aiming to explain the steering mechanism of the wasp ovipositor have been proposed [38–40]. According to one prevailing hypothesis, steering motion is achieved by selectively advancing the valves, thereby creating an offset at the tip, which, due to its beveled shape and off-axis

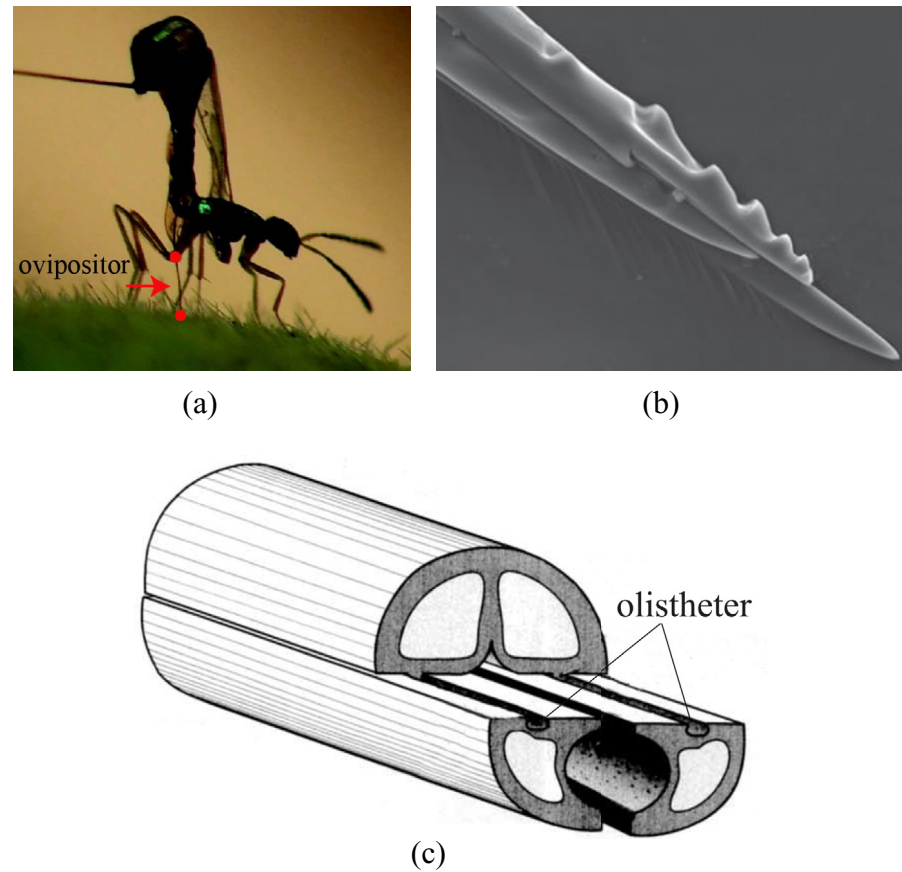
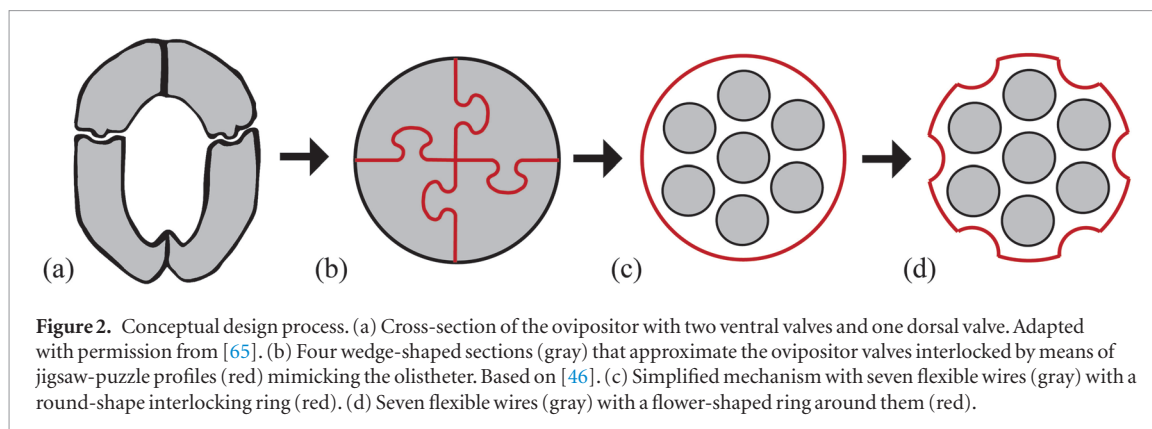


**Figure 1.** (a) Parasitoid wasp (*Apocrypta westwoodi*) ovipositing in a fig. Adapted with permission from [34]. (b) Scanning electron micrograph (SEM) showing the morphology of the ovipositor tip, with visible serrations on the surface. Adapted with permission from [34]. (c) Schematic representation of the ovipositor, with valves differentially protruding, held together by jigsaw-puzzle-like olistheters. Adapted with permission from [36].

reaction forces applied on it by the surrounding substrate, deflects [40].

The mechanism used by the wasp for advancing and steering inside solid substrates has inspired the design of a variety of devices, ranging from planetary and earth drills [41] to medical needles and probes [42]. Over the last decade, Rodriguez y Baena and coworkers have developed and tested a series of medical needles and probes inspired by the wasp ovipositor. Specifically, the steerable probe described by Frasson *et al* [42] consists of four segments connected with a jigsaw-puzzle interlocking mechanism similar to the olisthether in the wasp ovipositor. Each of the segments has a bevel-tip, so that when the segments are aligned, the needle tip has a conical shape. The segments are actuated independently from each other. First, one of the segments is moved forward, and due to off-axis reaction forces at the segment tip from the substrate, the segment deflects in the direction of the bevel. Then, the other segments are advanced, following the curved trajectory laid out by the first segment. The curvature of the probe can be controlled by changing the offset between the segment that is protruded and the rest of the probe, a steering principle called ‘programmable bevel-tip’ [43, 44]. Frasson *et al* [44] experimentally demonstrated that there is a linear relationship between the offset and the steering

curvature, and that for a probe with a larger diameter a larger offset is needed in order to achieve the same curvature as with a smaller probe. Extensive work has been also done on the optimization of the probe in terms of the geometry of the interlocking mechanism [45–47] and the surface topography of the probe [48–51]. Specifically, it was found that a small fin- or tooth-like outer-surface topography make the needle insertion easier compared to the use of smooth surfaces, while providing large gripping forces when the needle is retracted [48, 49]. The insertion into tissue by reciprocal motion of the segments has been tested [52–54], the probe-tissue interaction has been simulated with finite element methods [55], and control strategies for steering in three dimensions have been investigated [56]. A series of prototypes have been presented, with diameters of 12 mm [57], 8 mm [58], and 4 mm [59]. It was found that forward motion through soft substrates by means of reciprocal motion of the segments of the probe is possible, albeit limited to certain types of substrate materials, such as muscle and agar gel. In this case, teeth on the probe surface have been used to enable forward motion [52]. It has been further shown that reciprocal insertion could result in less tissue disruption and less target displacement than direct pushing of probe would cause [54, 60].



Sprang *et al* [61] presented an ovipositor-inspired needle consisting of four rigid longitudinal square segments and a total thickness of 2 mm that was advanced through gelatin with zero external pushing force. Sprang *et al*'s prototype did not bear serrations; instead, the dynamic friction force along the advancing segment and the force at the segment tip was compensated by the difference in contact area between the stationary and advancing segments. Only forward motion was investigated; the prototype was not designed for steering. Moreover, Sprang's needle did not contain an interlocking mechanism to hold the segments together; this design choice was due to difficult miniaturization of the required jigsaw-puzzle profiles. The lack of interlocking led to bifurcation of the four segments during propagation of the needle through the gel.

### 1.3. Aim

This work builds upon the existing studies on ovipositor-inspired steerable needles and probes and proposes a new design approach in order to develop a needle that uses a push-pull mechanism during both forward motion and steering. The needle steers without the need for axial rotation and has a diameter suitable for core needle biopsy and brachytherapy treatments. Specifically, we aimed for a needle diameter under 2 mm, that is, approximately 14 Gauge (G), considering that needles commonly used in core needle biopsy and brachytherapy have diameters of 14–19 G [62] and 17–18 G [63], respectively. We first present the design of the needle, followed by an experimental evaluation of the forward motion and steering performance of the needle. A preliminary version of this work has been briefly reported in [64].

## 2. Needle design

### 2.1. Conceptual design

#### 2.1.1. Shape of longitudinal segments

A direct technical analogue of the wasp ovipositor would be a needle consisting of four wedge-shaped sections arranged in such a way that altogether they form a circle. However, manufacturing long and well-aligned wedge-shaped sections in small dimensions

is technically challenging [46]. One way to bypass this issue is by reasoning that the wedge-shaped sections can be approximated by a set of cylindrical sections arranged in such a way that altogether they approximate a circle. Following this line of reasoning, we decided to use off-the-shelf round flexible metal wires as longitudinal segments (figure 2).

#### 2.1.2. Number of longitudinal segments

Choosing the number of wires is an optimization process between the number of steering directions, slip during forward motion, total diameter of the needle, and bending stiffness. Steering can be induced by selectively moving one or more of the wires forward, thereby creating radial asymmetry at the needle tip. The steering direction and angle can be varied by choosing different combinations of wires to protrude and different offsets. Theoretically, omnidirectional steering is possible with a minimum of four wires; however, increasing the number of wires allows for a larger number of steering directions. With respect to slip during forward motion, it has been previously shown that the higher the ratio between the number of stationary and moving longitudinal segments, the lower the slip [61], thereby the smaller the lag between the actual and desired insertion depth. In other words, a larger number of wires allows for a larger number of steering directions and for lower slip in forward motion. On the other hand, for a constant diameter of the wires, the diameter and bending stiffness of the needle increases with the number of wires. Moreover, a larger diameter implies greater invasiveness of the medical procedure and more tissue damage.

In our study, we selected the number of wires that would allow us to investigate whether forward motion and steering of a needle consisting of multiple untreated wires (i.e. no bevel-tip or microtextured surface) is viable. A total of five wires would have been enough to create an asymmetry between advancing wires while maintaining a ratio of stationary to advancing wires greater than one. However, in order to allow steering in two perpendicular planes, we opted for six wires, concentrically arranged around a seventh central stabilizing wire (figure 2).

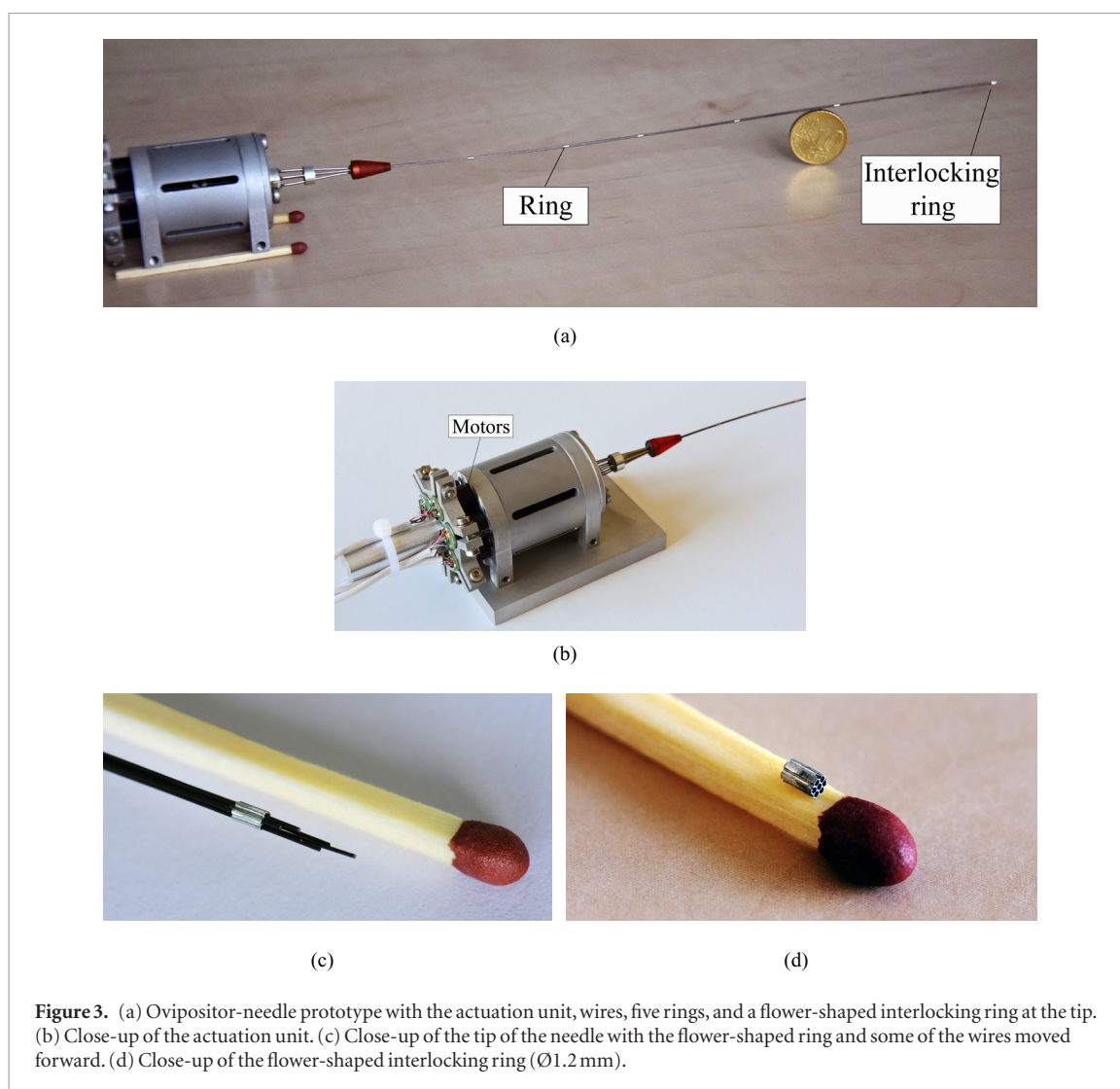


**Figure 3.** (a) Ovipositor-needle prototype with the actuation unit, wires, five rings, and a flower-shaped interlocking ring at the tip. (b) Close-up of the actuation unit. (c) Close-up of the tip of the needle with the flower-shaped ring and some of the wires moved forward. (d) Close-up of the flower-shaped interlocking ring ( $\text{\O}1.2\text{ mm}$ ).

### 2.1.3. Interlocking mechanism

As mentioned in section 1.2, the ovipositor valves are interlocked by the olistheter, a jigsaw-puzzle like structure, which allows the valves to slide along each other, avoiding their separation. Frasson *et al* [46] and Burrows *et al* [59] used a similar structure in their  $\text{\O}12\text{ mm}$  and  $\text{\O}4\text{ mm}$  prototypes. However, miniaturization of such a complex interlocking mechanism is challenging from a manufacturing perspective. To develop a needle with a diameter under 2 mm, we decided to step away from nature and to interlock the wires externally using an interlocking ring with seven holes through which the wires are fed. We adjusted the ring shape to a flower-shape to reduce the resistance with the substrate (figure 2).

## 2.2. Needle prototype

The ovipositor-inspired needle prototype consists of seven superelastic nickel titanium (NiTi) wires with a diameter of 0.25 mm and a length of 160 mm. The diameter of 0.25 mm was chosen as it was the smallest available for the material characteristics required (i.e. straightened NiTi wires). Six wires can slide independently from each other along the length of the needle and are concentrically arranged around

the seventh wire, which is fixed at the needle base. The wires are straight at room temperature and have a smooth surface.

Two types of rings are used to hold the wires together: the flower-shaped interlocking ring and five standard rings (figure 3). The flower-shaped interlocking ring (aluminum,  $\text{\O}1.2\text{ mm}$ , 2.0 mm long) aligns the wires and keeps them together. The ring has seven holes through which the wires are fed: one central hole and six outer holes arranged in a circle with a radius of 0.38 mm. The central wire is glued to the central hole, whereas the six outer wires can slide through the outer holes. The diameter of the holes is 0.3 mm, letting the 0.25-mm wires move freely inside the ring.

In order to avoid buckling of individual wires during the actuation and to keep all the wires together along the full length of the needle, five stainless steel rings ( $\text{\O}_{\text{in}}\text{ }0.9\text{ mm}$ ,  $\text{\O}_{\text{out}}\text{ }1.0\text{ mm}$ , 2.0 mm long), uniformly spaced between the base of the needle, are used. The total diameter of the needle is 1.2 mm at the tip, which corresponds to the outer diameter of the interlocking ring. The body of the needle has a diameter of 0.75 mm.

Each of the six movable wires is connected to a slider that is moved backward and forward by a bipo-

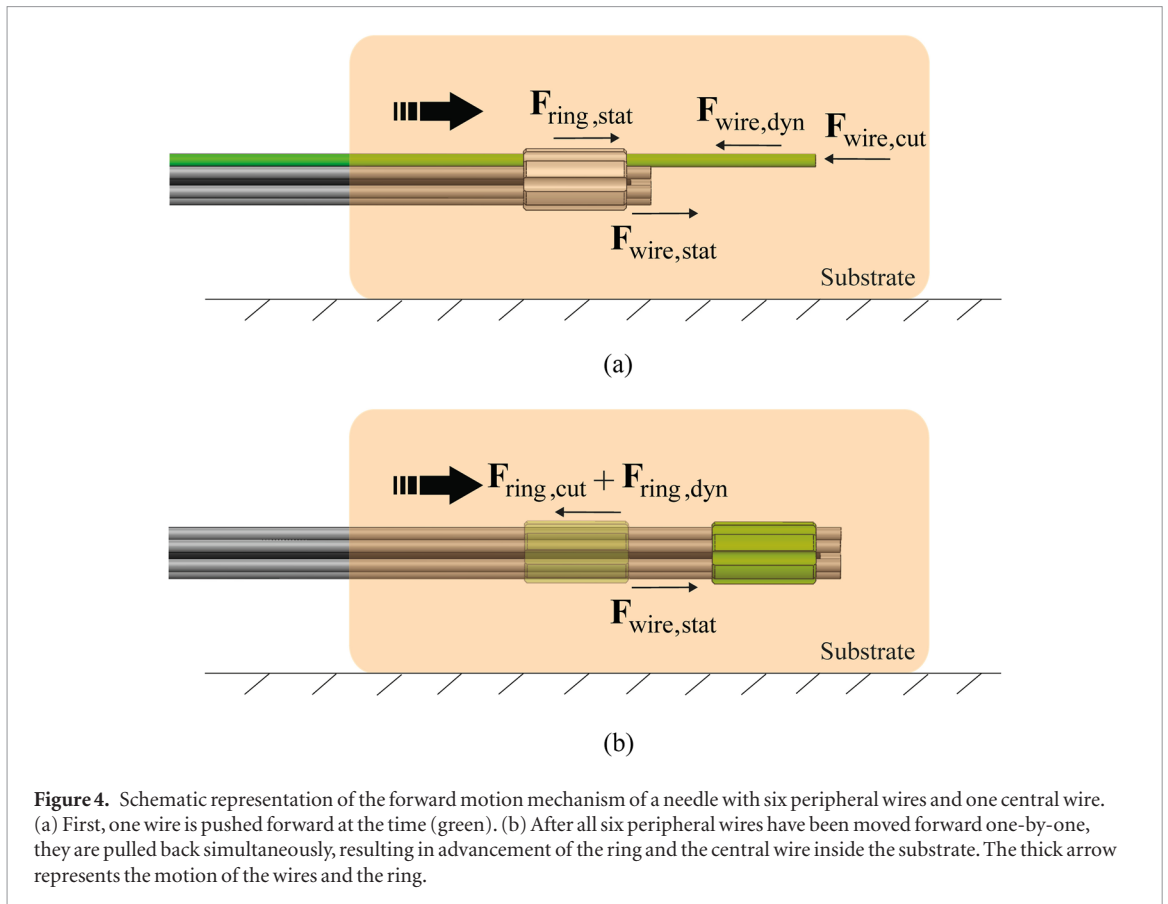


**Figure 4.** Schematic representation of the forward motion mechanism of a needle with six peripheral wires and one central wire. (a) First, one wire is pushed forward at the time (green). (b) After all six peripheral wires have been moved forward one-by-one, they are pulled back simultaneously, resulting in advancement of the ring and the central wire inside the substrate. The thick arrow represents the motion of the wires and the ring.

lar stepper motor AM0820 with step angle  $18^\circ$  (Faulhaber, Germany) in conjunction with a leadscrew (M2, 28 mm long). The stepper motors and leadscrews are placed in an aluminium housing. A stepper motor combined with a leadscrew-slider mechanism was chosen, in order to achieve a linear motion of the wires. Linear motion could have also been achieved by means of linear actuators, but those are usually bulky. The maximum travel distance of each slider and thus of the needle wires is 20 mm. The six stepper motors are actuated using six stepper drivers DRV8834 (Texas Instruments, TX) and an Arduino MEGA 2560 micro-controller.

### 2.3. Forward motion and steering of the needle

#### 2.3.1. Forward motion

The needle is moved forward through the substrate by first pushing the six wires one-by-one or two-by-two, followed by pulling on all six wires simultaneously, which advances the interlocking ring and the central wire into the substrate. This two-phase motion sequence will henceforth be referred to as a ‘cycle’.

Figure 4 shows the forces acting on the needle prototype during the forward motion. Assume the general case in which  $m$  wires move forward and  $n$  wires are stationary. The motion of a single wire can be expressed as the sum of the external force  $F_{ext}$  (i.e. pushing), the friction force along the length of the wire in contact with the substrate  $F_{wire,fric}$ , the cutting force acting at the tip  $F_{wire,cut}$ , and the static friction between the interlocking ring and the substrate  $F_{ring,stat}$ . If we

consider a total of  $m+n$  wires, using the Newton’s second law we get:

$$\sum_{i=1}^{m+n} (F_{ext,i} + F_{wire,fric,i} + F_{wire,cut,i}) + F_{ring,stat} = \sum_{i=1}^{m+n} m_{wire,i} a_{wire,i} \quad (1)$$

where  $m_{wire}$  is the mass of the wire and  $a_{wire}$  is its acceleration. As shown in previous studies [53, 61] the needle can move forward with a zero net external force ( $\sum F_{ext} = 0$ ) or (even) a net pulling force ( $\sum F_{ext} < 0$ ):

$$\sum_{i=1}^{m+n} F_{ext,i} = - \sum_{i=1}^m (F_{wire,dyn,i} + F_{wire,cut,i}) - \sum_{i=1}^n F_{wire,stat,i} - F_{ring,stat} + \sum_{i=1}^{m+n} m_{wire,i} a_{wire,i} \leq 0 \quad (2)$$

where  $F_{wire,dyn}$  is the dynamic friction force acting on the moving wire, and  $F_{wire,stat}$  is the static friction force acting on the static wires; there are no forces acting at the tip of the static wires. Assuming that the inertia term is negligibly small, and in order for the  $m$  wires to move forward, the sum of the dynamic friction force and the cutting force of the wires moving forward should be smaller than the static friction force of the  $n$  stationary wires and the interlocking ring, that is:

$$- \sum_{i=1}^m (F_{wire,dyn,i} + F_{wire,cut,i}) \leq \sum_{i=1}^n F_{wire,stat,i} + F_{ring,stat} \quad (3)$$

In the second phase of the actuation cycle, in which all  $m+n$  wires are pulled simultaneously, the cutting and dynamic friction force of the advancing interlock-

ing ring should be compensated by the static friction force between the wires and the substrate, that is:

$$\mathbf{F}_{\text{ring,cut}} + \mathbf{F}_{\text{ring,dyn}} \leq \sum_i^{m+n} \mathbf{F}_{\text{wire,stat},i} \quad (4)$$

where  $\mathbf{F}_{\text{ring,cut}}$  and  $\mathbf{F}_{\text{ring,dyn}}$  are the cutting force and the dynamic friction force of the interlocking ring, respectively. By repeating this actuation cycle, the needle advances inside the substrate. If any of the two inequalities is not satisfied, the needle slips.

### 2.3.2. Steering

Each needle wire has a flat (rather than bevel) tip, therefore the first step for steering is to generate an asymmetry at the needle tip. This is done by inducing an offset (henceforth called bevel offset,  $BO$ ) between a pair of adjacent needle wires. We call this configuration ‘discrete bevel-tip’, since it is a tip made out of multiple single segments that approximate a bevel-tip (figure 5(c)). With a discrete bevel-tip it is possible to create various bevel angles. For example, by moving a wire forward over an offset  $BO_1$  a bevel angle  $a_1$  is generated (figure 5(h)), whereas by moving a wire over an offset  $BO_2 > BO_1$  a bevel angle  $a_2 < a_1$  is generated (figure 5(i)). Steering could be achieved with the following actuation scheme. First, a  $BO$  is set between two adjacent wires, and this discrete bevel-tip is advanced to a predefined distance (henceforth called stroke,  $S$ ), deflecting and laying a curved path in the substrate. Next, a  $BO$  is set between the two adjacent wires that are consecutive to the first pair of wires, and this second discrete bevel-tip is advanced for  $S$ , reinforcing the curved path laid by the first pair. Then, the remaining two wires are advanced over  $S$ , following the curved path laid by the other two pairs (figure 5). Finally, all six wires are pulled simultaneously backwards, so that the seventh (central) wire and the interlocking ring move forward along the curved trajectory. The steering direction is determined by the pair of wires used to form the discrete bevel-tips. For example, steering to the left is achieved by creating a discrete bevel-tip between wires 1 and 6 (with wire 6 protruding by a distance  $BO$  with respect to wire 1) and a second discrete bevel between wires 4 and 5 (with wire 5 protruding by a distance  $BO$  with respect to wire 4) (figure 5). Similarly, steering to the right is achieved by creating a discrete bevel-tip between wires 1 and 2 and a second bevel-tip between wires 3 and 4.

## 3. Materials and methods

The performance of the needle prototype was evaluated in two experiments. In experiment 1 we evaluated the performance of the prototype in forward motion, and in experiment 2 we evaluated the steering performance. The experimental setup was the same for both experiments.

### 3.1. Experimental setup

The experimental setup consisted of the actuation unit as described in section 2, a test rig, and data acquisition systems (figure 6(a)). The actuation unit was mounted on an aluminum base plate using four bolts. A lightweight aluminum cart ( $210 \times 50$  mm, 28 g) mounted to four wheels was designed to carry a gelatin phantom (Dr. Oetker).

The gelatin phantoms were prepared by mixing gelatin powder with water heated at 70–80 °C. The liquid gelatin was poured into containers and stored overnight at 5 °C. A new batch of gelatin was prepared for each day of the experiments. A gelatin block of  $50 \times 170 \times 30$  mm (width  $\times$  length  $\times$  height) was cut and placed on the cart for each experimental trial.

An alignment ring (aluminum,  $\varnothing$  3.0 mm, 2.0 mm long) was added to the body of the needle and fixed to the cart (figure 6(b)). The alignment ring contained seven holes and had an asymmetric cross-section to ensure that the needle was radially aligned along its length. The wires could freely slide through the seven holes of the alignment ring.

In our experiments, instead of moving the needle and its actuation unit toward the gelatin cart, the actuation unit was fixed; actuating the needle resulted in moving the gelatin cart toward the actuation unit. The rolling motion of the four wheels was laterally constrained by a groove in the base plate, and the rolling friction of the wheels was negligible. A millimeter graph paper was placed at the bottom surface of the cart to give a reference to the needle deflection during the experiments. A laser proximity sensor (MicroEpsilon optoNCDT1302-200, range: 200 mm, resolution: 0.1 mm) was used to record the position of the cart. The laser sensor data were collected using a data acquisition unit (NI USB-6211, 16-bit) in conjunction with LabVIEW 2013 at a sampling frequency of 5 Hz.

Next to the recording of the position of the cart, in experiment 2 the experimental trials were recorded using a video camera (HC-V250, Panasonic, Osaka, Japan). Moreover, at the end of each experimental trial of experiment 2 a top-down view photograph of the needle inside the gelatin phantom was taken with a camera (Nikon D750, Tokyo, Japan) mounted on a tripod, in order to define the final curvature of the needle. The position of the camera was calibrated with a spirit level to ensure that it was orthogonal to the table where the needle and the cart were placed.

For all experimental trials of both experiments, 4% weight of gelatin powder in water was used. A Young’s modulus of 4.65 kPa was measured for this gelatin phantom by means of dynamic mechanical analysis (PerkinElmer Instruments, amplitude = 40  $\mu$ m, frequency = 1 Hz, parallel plate geometry with 20 mm diameter), which corresponds to brain tissue elasticity (2.7–5 kPa [66]). The combined weight of the cart and gelatin phantom was kept constant for all trials

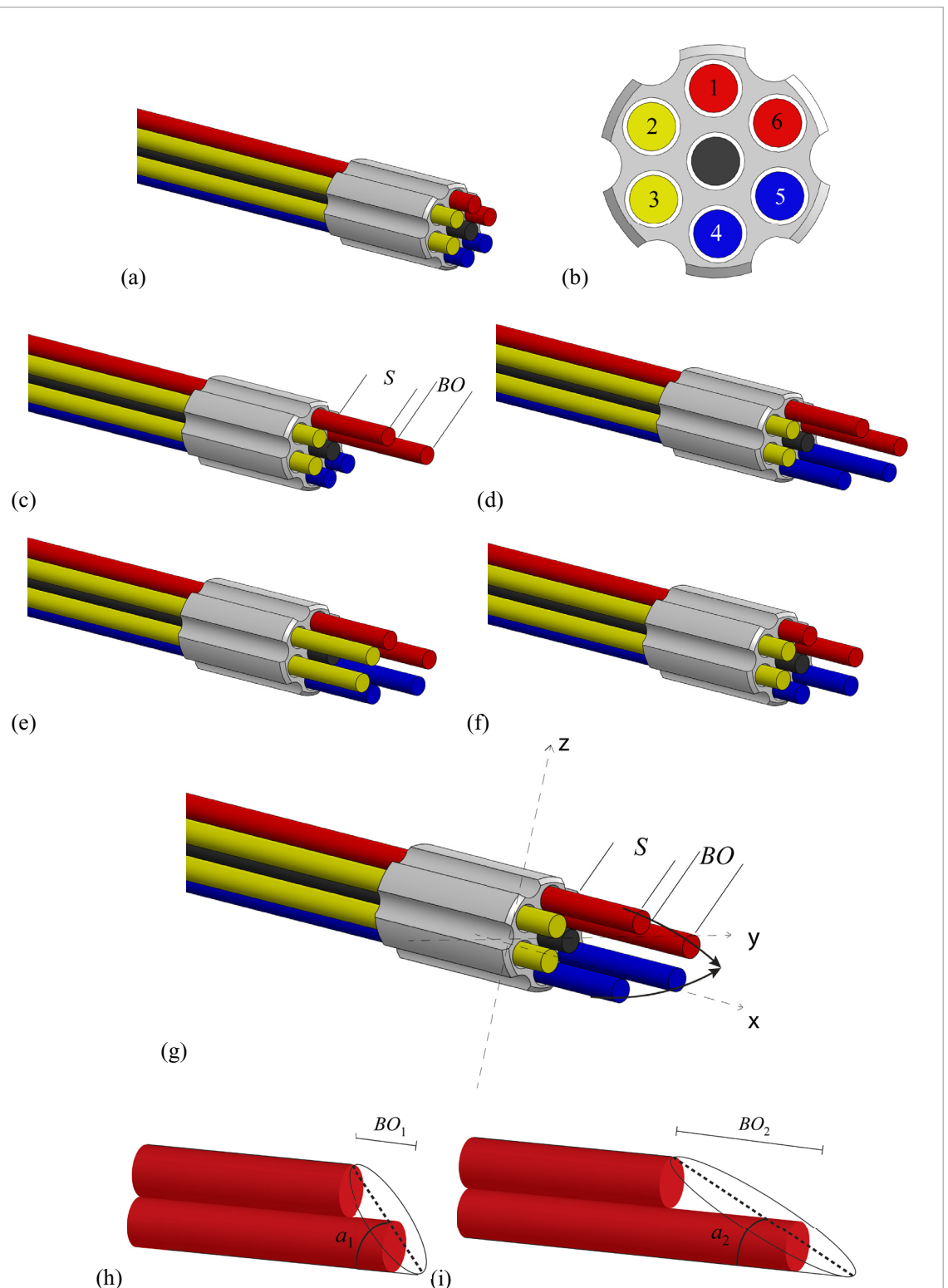


**Figure 5.** (a) Initial position of the wires. (b) Cross-section of the needle. (c)–(f) Steps of the actuation cycle. Steering to the left is achieved by creating a first discrete bevel between wires 1–6 (red), with wire 6 protruding by bevel offset ( $BO$ ) with respect to wire 1. (c) The two wires are then advanced to the desired stroke ( $S$ ). (d) A second discrete bevel is created between wires 5–4 (blue), with wire 5 protruding with the same  $BO$  and moves for  $S$ . (e) Wires 3–2 are then pushed forward for  $S$  (yellow). (f) Lastly, all six wires are pulled to let the ring advanced. (g) Schematic representation of the needle tip showing the steering mechanism. (h) Discrete bevel-tip with angle  $a_1$  and  $BO_1$ . (i) Discrete bevel-tip with angle  $a_2$  and  $BO_2$ . In this example,  $BO_2 > BO_1$ . A large  $BO$  corresponds to a small angle, that is,  $a_2 < a_1$ .

(mean = 214.66 g, standard deviation = 1.69 g). The needle segments were actuated at a speed of  $2 \text{ mm s}^{-1}$ . The total number of cycles executed by the Arduino software was chosen to result in a theoretical needle insertion depth of 120 mm in all experimental trials

of both experiments. Each trial was conducted with a specific stroke (see section 3.2.2 and section 3.3.2), and during each actuation cycle the wires were moved forward over that stroke. The number of cycles equaled the ratio of 120 mm over the stroke.

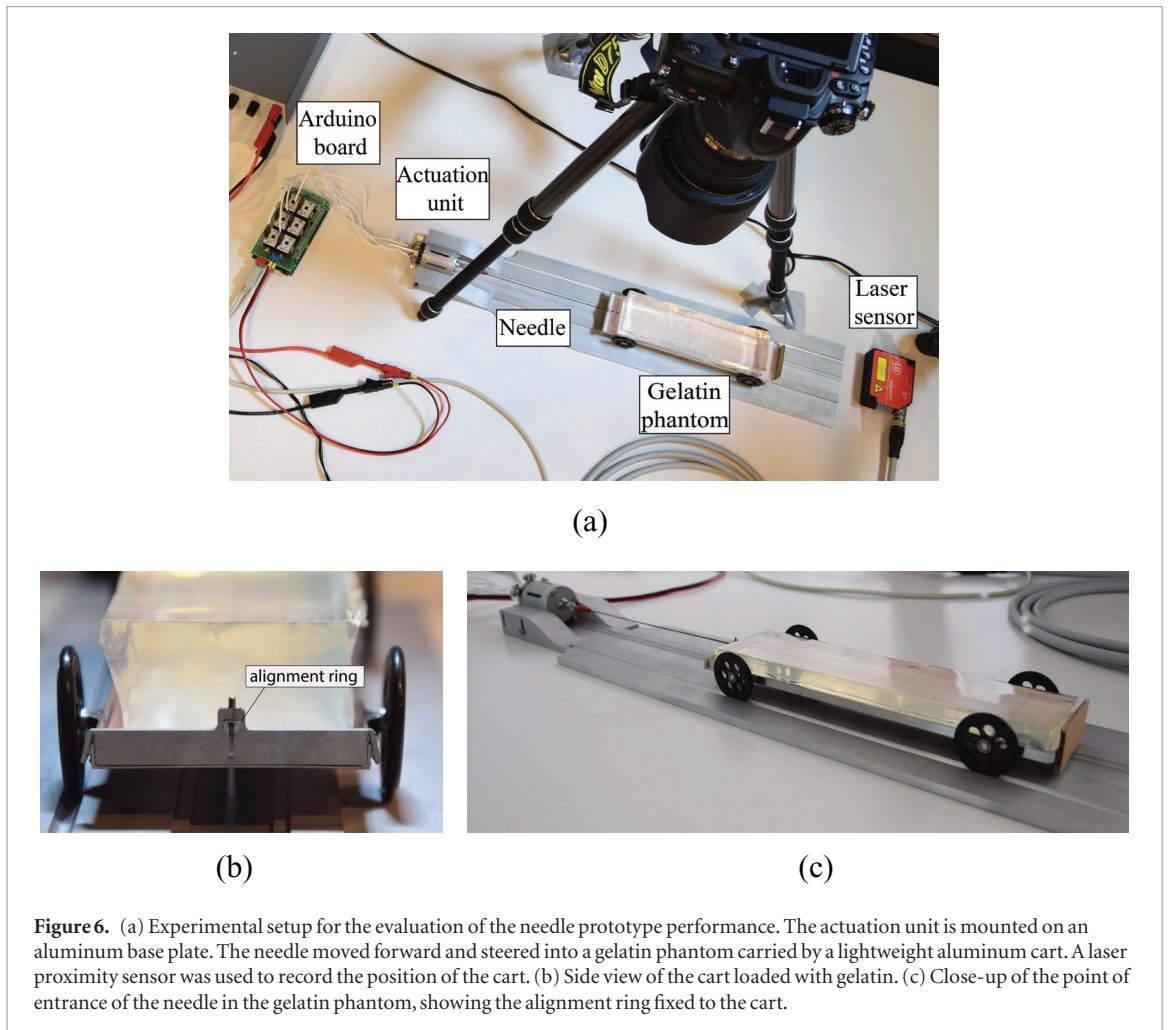


**Figure 6.** (a) Experimental setup for the evaluation of the needle prototype performance. The actuation unit is mounted on an aluminum base plate. The needle moved forward and steered into a gelatin phantom carried by a lightweight aluminum cart. A laser proximity sensor was used to record the position of the cart. (b) Side view of the cart loaded with gelatin. (c) Close-up of the point of entrance of the needle in the gelatin phantom, showing the alignment ring fixed to the cart.

### 3.2. Experiment 1—forward motion

#### 3.2.1. Hypothesis

We expected the slip of the needle during forward motion to be inversely proportional to the ratio of the number of stationary to moving needle wires. That is, the slip is expected to increase with the number of simultaneously actuated wires, in line with Sprang *et al* [61].

#### 3.2.2. Dependent and independent variables

The dependent variable in experiment 1 was the slip between the needle and the gelatin. We define slip as the ratio of the measured insertion depth to the theoretical insertion depth of the needle. The independent variable was the number of wires that were actuated simultaneously, either one (single actuation) or two (paired actuation). Stroke  $S$  was set to 4.0 mm for both single and paired actuation trials.

#### 3.2.3. Experimental procedure

A gelatin block was placed on the cart, and the needle was manually inserted about 25 mm into the gelatin (starting position) to reduce the effects of cutting and friction forces acting on the tip during punching of the substrate. The desired actuation setting (single or paired actuation) was entered in the Arduino software, the laser sensor was switched on, and the needle wires were actuated. The needle wires were actuated

counterclockwise, starting with wire 1 in single actuation and with wires 1–2 in paired actuation. At the end of each trial the needle was removed from the phantom and cleaned with warm water. A new gelatin phantom was used for each trial. Six trials were conducted for each actuation condition (single versus paired), in a randomized order. All measurements were conducted over the course of one day.

#### 3.2.4. Data analysis

The raw data of the cart position collected by the laser sensor were imported and processed in MATLAB (version 2014b). The slip ratio *slip* was calculated as

$$slip = 1 - \frac{d_{meas}}{d_{theor}}, \quad (5)$$

where  $d_{theor}$  is the theoretical insertion depth for each cycle and  $d_{meas}$  is the measured insertion depth for each cycle, calculated by the difference between the position of the cart at the starting point of two consequential actuation cycles

$$d_{meas} = p_{a+1} - p_a, \quad (6)$$

where  $a$  is the number of an actuation cycle, and  $p$  is the position of the cart. For estimating slip, we assumed that the advancing needle did not deviate from the straight path.

### 3.3. Experiment 2—steering

#### 3.3.1. Hypothesis

We hypothesized that the steering curvature of the needle is proportional to the bevel offset  $BO$ , consistent with experimental and analytical studies on bevel-tip needles showing that smaller bevel angles lead to larger steering curvatures [67, 68]. For a given  $BO$  we further expected a proportional relationship between steering curvature and stroke  $S$ , as  $S$  can be compared to the length of a cantilever beam subjected to a load at its tip.

#### 3.3.2. Dependent and independent variables

The dependent variable was the steering curvature of the needle. The independent variables were  $BO$ ,  $S$ , and the steering direction.  $BO$  was varied between 0.9, 1.8, and 3.6 mm, resulting in bevel angles of about 20, 10, and 5 degrees respectively.  $S$  was varied between 2.0, 4.0, and 6.0 mm. The steering direction was varied either left or right.

#### 3.3.3. Experimental procedure

From the 18 possible combinations ( $3 BO \times 3 S \times 2$  steering directions), a set of 10 conditions was chosen, so that  $BO$  was varied for a constant  $S = 4.0$  mm, and  $S$  was varied for a constant  $BO = 3.6$  mm, for both steering directions. The stroke value of 4.0 mm was chosen because it was expected that it would result in higher steering curvatures than a stroke of 2.0 mm, while keeping the needle wires closer to each other than a stroke of 6 mm. The bevel offset value of 3.6 mm, which corresponds to the smallest bevel angle, was chosen because it was expected that the curvature increases with small bevel angles [69]. For steering to the left, the wire pairs were actuated clockwise, starting with the wire pair 6–5. For steering to the right, the wire pairs were actuated counterclockwise, starting with the wire pair 1–2. The same experimental procedure was followed as in experiment 1. Each condition was repeated five times, resulting in a total of 50 trials. All trials were conducted in a randomized order over the course of eight days.

#### 3.3.4. Data analysis

The photographs of the final position of the needle inside the gelatin were cropped to exclude the 25 mm of the initial manual insertion. Then the MATLAB image processing toolbox was used to convert the photographs into binary images, after which the needle shape and centerline were extracted. Next, a circle was fitted to the needle centerline based on the circle equation in one plane

$$x^T \cdot x + b^T \cdot x + c = 0, \quad (7)$$

where  $x, b \in R^2$ . Using the extracted needle data points ( $x$ ), the fitted circle radius  $r_{\text{fit}}$  was obtained for each experimental trial, and the curvature  $k$  was calculated as

$$k = (r_{\text{fit}})^{-1}, \quad (8)$$

where  $k$  was obtained assuming that the needle moved only in one plane. For the trials in which steering was not achieved, we set  $k$  to 0.

In addition, the deflection-to-insertion ratio  $d/i$  was estimated by extracting the initial and end distance from the centerline to calculate the deflection  $d$  of the needle from the straight path and by dividing  $d$  with the insertion depth  $i$ .

## 4. Results

### 4.1. Experiment 1—forward motion

One dataset of the single actuation trials was removed because the laser sensor data were erroneous. The mean value of slip was 0.21 for single actuation ( $n = 5$ ) and 0.34 for paired actuation ( $n = 6$ ) (figure 7). In figure 7 it can be seen that the variability in slip across trials was greater in the paired actuation than in the single actuation. In both single and paired actuation, slip was highest in the first cycles and stabilized after about nine cycles. The mean total insertion depth of the needle in the single actuation trials was 94.6 mm ( $n = 5$ ) and 79.4 mm in paired actuation ( $n = 6$ ).

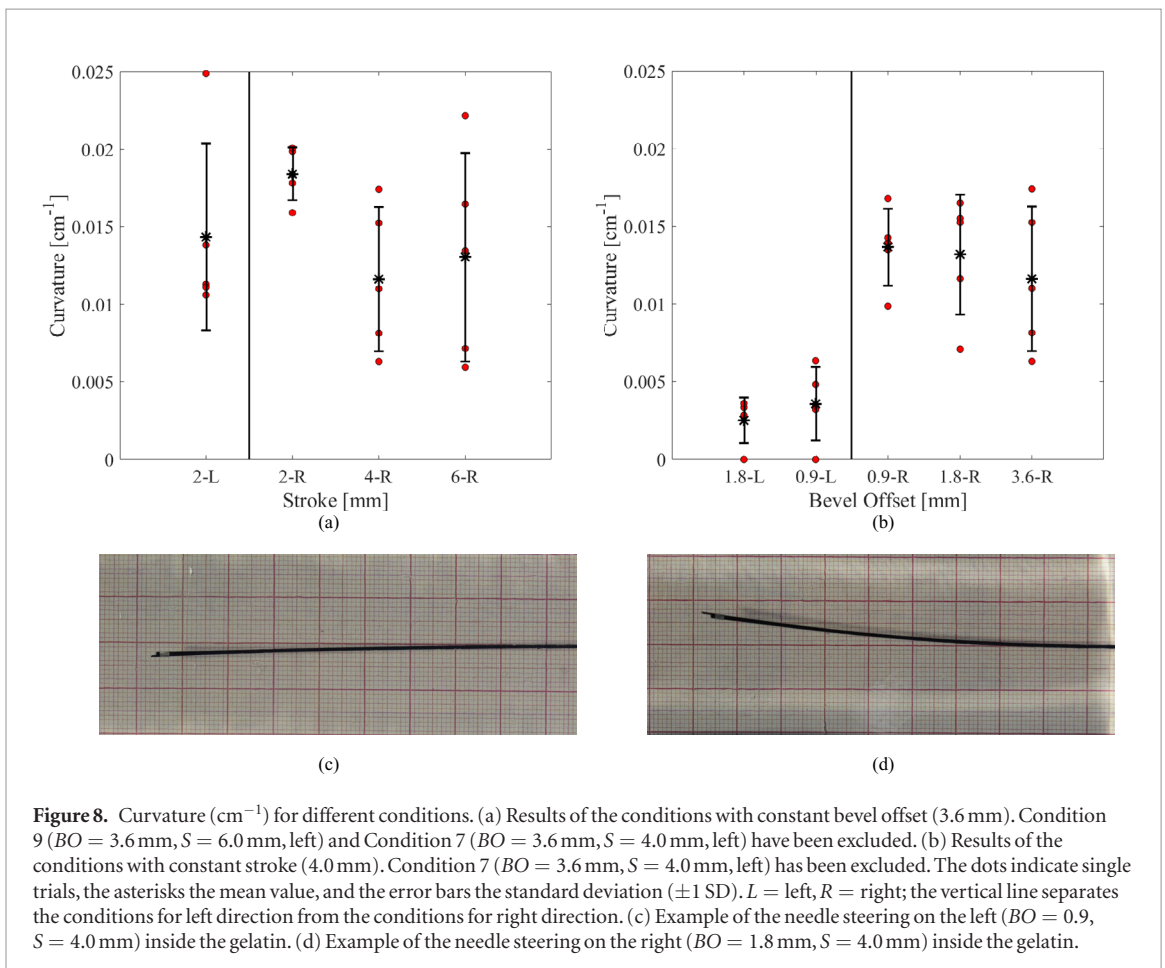
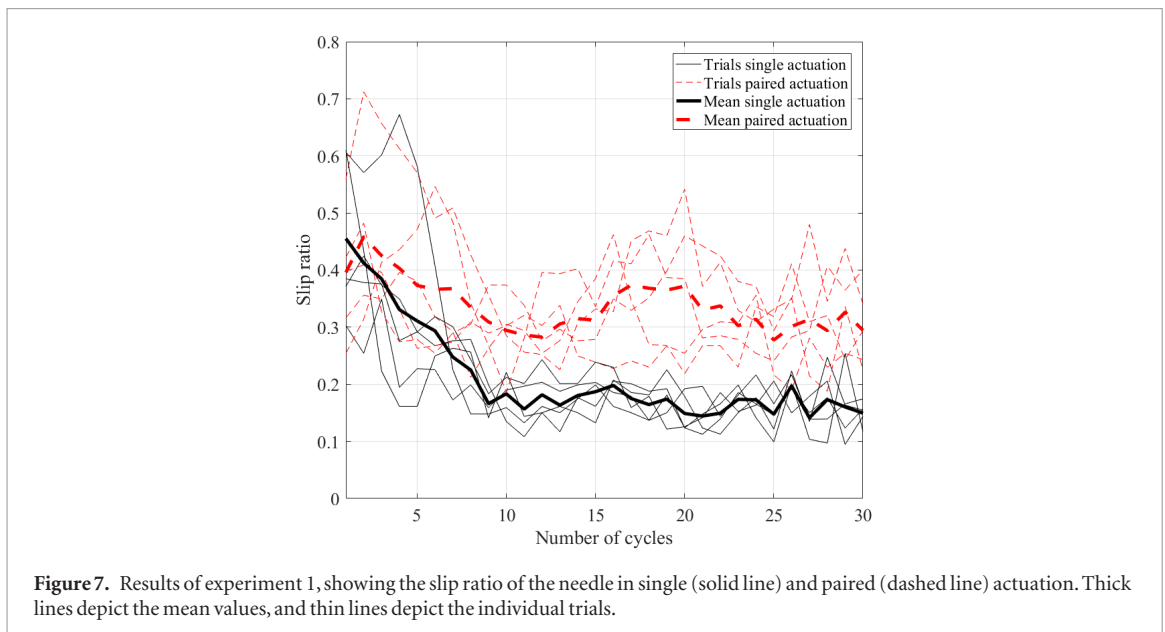
### 4.2. Experiment 2—steering

Steering to the left was unsuccessful (i.e. steering in the opposite direction or not steering at all) in 10 out of the 25 trials. Eight of the ten failed tests occurred while steering with a high  $BO$  and  $S$ . Specifically, in both Conditions 7 ( $BO = 3.6$  mm,  $S = 4.0$  mm) and 9 ( $BO = 3.6$  mm,  $S = 6.0$  mm), four out of the five trials showed steering in the opposite direction; these two conditions were excluded from further analysis. In each of Conditions 3 ( $BO = 1.8$  mm,  $S = 4.0$  mm) and 5 ( $BO = 0.9$  mm,  $S = 4.0$  mm), one trial showed no steering; the curvature for these two trials was set to 0. Steering to the right was successful (i.e. steering to the right direction) in all trials.

Steering curvatures were larger for steering to the right than for steering to the left (figure 8). The standard deviation across trials of the same condition increased with increasing  $BO$  and  $S$  when steering to the right. The largest mean curvature ( $k = 0.0184 \text{ cm}^{-1}$ ) was achieved for Condition 2 ( $BO = 3.6$  mm,  $S = 2.0$  mm, steering direction = right). Figure 9 shows the deflection-to-insertion ratio for each condition. Ratios were higher for steering to the right than for steering to the left. The highest deflection-to-insertion ratio (0.0778; mean across 5 trials) was achieved for Condition 10 ( $BO = 3.6$  mm,  $S = 6$  mm, steering direction right). Table 1 shows the mean curvature values and corresponding standard deviations for each condition (for a video of the needle steering inside the gelatin phantom see supplementary material ([stacks.iop.org/BB/13/016006/mmedia](https://stacks.iop.org/BB/13/016006/mmedia))).

## 5. Discussion

In this study, we presented a novel design of a steerable needle inspired by the ovipositor of parasitoid wasps. Preventing buckling through zero external pushing force and steering by means of a reconfigurable tip are



two features of the wasp ovipositor that have already been incorporated in earlier steerable needle designs showing promising results [53, 61]. While previous work has mainly been directed toward probes for neurosurgery with a minimum diameter of 4 mm [59], the goal of our study was to develop a needle that utilizes the ovipositor mechanism while having

a diameter under 2 mm, so that it can be used in percutaneous procedures, such as brachytherapy and core needle biopsy.

### 5.1. Needle design

With a diameter of 1.2 mm, the prototype presented here is thinner than other ovipositor-inspired needles

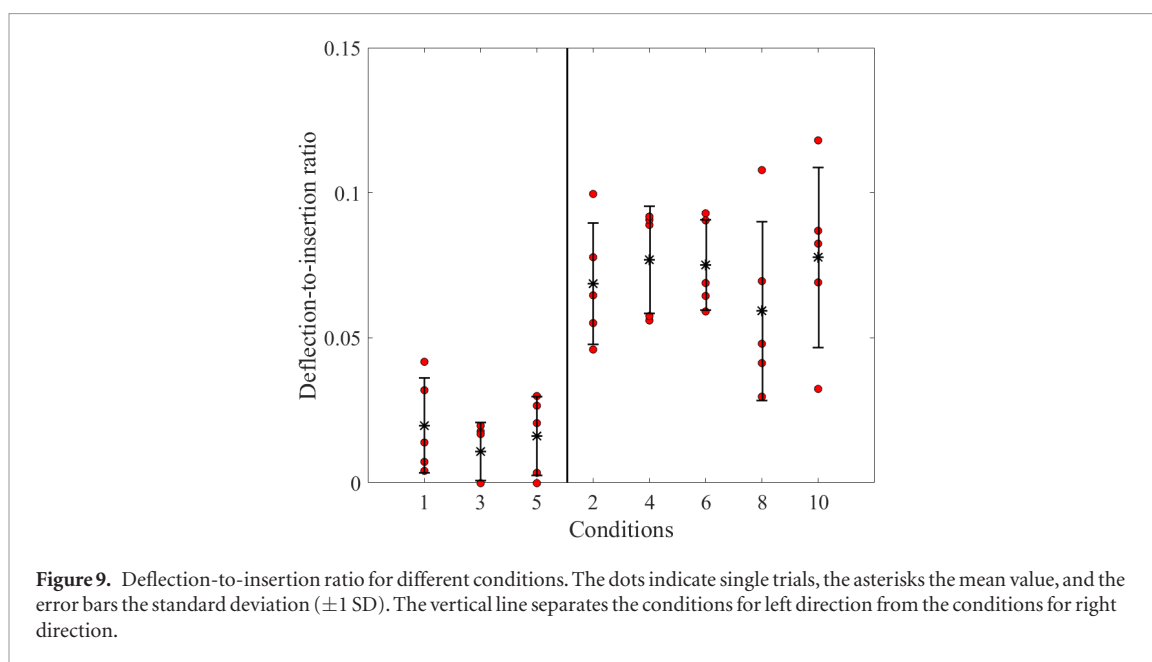


**Table 1.** Experimental conditions and curvature mean values for experiment 2.

Condition	BO (mm)	S (mm)	Steering direction	$k$ ( $\text{cm}^{-1}$ ) (mean $\pm$ std)	$d/i$ (no unit) (mean $\pm$ std)
1	3.6	2.0	Left	$0.0143 \pm 0.0060$	$0.0198 \pm 0.0163$
2	3.6	2.0	Right	$0.0184 \pm 0.0017$	$0.0686 \pm 0.0209$
3	1.8	4.0	Left	$0.0025 \pm 0.0014$	$0.0108 \pm 0.0099$
4	1.8	4.0	Right	$0.0132 \pm 0.0039$	$0.0769 \pm 0.0185$
5	0.9	4.0	Left	$0.0036 \pm 0.0024$	$0.0161 \pm 0.0136$
6	0.9	4.0	Right	$0.0137 \pm 0.0025$	$0.0751 \pm 0.0155$
7	3.6	4.0	Left	N/A	N/A
8	3.6	4.0	Right	$0.0116 \pm 0.0047$	$0.0592 \pm 0.0308$
9	3.6	6.0	Left	N/A	N/A
10	3.6	6.0	Right	$0.0130 \pm 0.0067$	$0.0778 \pm 0.0310$

*Note.* BO = bevel offset; S = stroke;  $k$  = curvature;  $d/i$  = deflection-to-insertion ratio; N/A = condition excluded from the analysis because four out of five trials showed steering in the opposite direction.

and probes in the literature, which range between 4 and 12 mm [57–59]. This small diameter was achieved by using flexible wires as needle segments instead of wedge-shaped sections. The use of wires allows for a circular needle without the manufacturability challenges of creating cylindrical sections. We used an external interlocking mechanism placed at the tip, instead of internal interlocking of the segments [45], as the latter is difficult to manufacture in small dimensions. We showed that a push-pull mechanism, previously only tested in forward motion [61], can also be exploited during steering, preventing buckling while moving in a curved trajectory and thus improving the controllability of the needle motion. Moreover, instead of a bevel-tip, we proposed a steering mechanism that relies on the creation of a ‘discrete’ bevel between adjacent segments; such a configuration-based asymmetry allows to overcome manufacturability challenges in creating a bevel in small dimensions. Moreover, a discrete bevel-tip is dynamically variable, which might allow for more

accurate control of the steering direction of the needle as compared to a needle with a fixed bevel. Changing the direction of steering without the need of axial rotation prevents the generation of torsional stress on the needle body and therefore prevent angular lag between the orientation of the needle base and the needle tip [70]. This way of steering can facilitate the control of the needle tip and decrease the risk of tissue damage [23].

In summary, in this prototype, a series of novel aspects has been introduced and tested: (1) the use of flexible Nitinol wires, which allows for developing a needle with a small diameter without the need of manufacturing cylindrical sectors; (2) the use of external interlocking, which is arguably simpler to fabricate than an internal interlocking mechanism; (3) a new method of steering, in which beveled components are not needed; instead, a type of ‘discrete’ bevel is created by the configuration of the wires; (4) push-pull advancement during steering, which prevents buckling while in a curved trajectory.

## 5.2. Experiment 1—forward motion

Experiment 1 showed that needle slip was lower in single than paired actuation (0.21 versus 0.33), consistent with our hypothesis and previous work [61]. The slip values in our work are considerably lower than the mean slip of 0.7 reported in Sprang *et al* [61]. The difference in slip between the two studies might be attributed to the fact that Sprang *et al* used a stiffer gel (8 versus 4 wt%) and needle segments with larger diameter (0.5 versus 0.25 mm) than we did. A stiffer gel and a thicker needle both increase the forces at the tip of the needle, resulting to higher slip. Previous work has indeed shown that peak axial needle insertion force increases with needle size [71].

The slip ratio was higher at the beginning of the trial and stabilized after about nine cycles, which indicates that a certain initial insertion depth (of about 25 mm) is needed for the needle to move forward with constant slip. We conducted an additional experiment with five trials in which the initial needle insertion was 50 mm and found that for this initial insertion depth, the slip ratio was constant throughout the measurement. This result is consistent with previous studies having shown that during needle insertion, the friction force on the needle increases with insertion depth while the approximate cutting force stays constant [72]. We can expect that an equilibrium is reached at a certain depth between the static friction of the stationary wires and interlocking ring and the dynamic friction and cutting forces of the advancing wires, see also equation (3).

The greater variability in slip between trials observed in the paired actuation as compared to the single actuation can be due to the random deflection of the wires once they are advanced inside the gelatin. In paired actuation, the two wires that are moved forward simultaneously can either stay close to each other or separate from each other (i.e. bifurcate) as they move out of the flower shaped interlocking ring. Bifurcating wires are likely to result in higher friction as compared to trials in which the two wires stay together. Bifurcation was also observed in Sprang *et al* [61], in which the needle parts were not interlocked.

## 5.3. Experiment 2—steering

Needle steering is achieved by creating an offset between a pair of adjacent needle wires, which we call a ‘discrete bevel-tip’. This concept is similar to the ‘programmable bevel’ concept shown in Ko *et al* [57], where steering was achieved by creating an offset between the needle part and pushing the needle inside a gelatin phantom. A difference between the concepts of a discrete bevel-tip and a programmable bevel is that in the former, the needle is not directly pushed inside the gelatin; instead the insertion is achieved by a push and pull actuation sequence that, combined with the tip asymmetry, results in a curved path. A second difference is that the programmable bevel needle design presented

by Ko *et al* [57] consists of needle parts with a fixed bevel-tip, whereas in our design the needle parts have a flat tip and the bevel is created by making an offset between them, which means that the bevel angle can be altered.

From the results of experiment 2 we did not find a systematic effect of *BO* on curvature. It is known that needle deflection increases when the bevel angle decreases [69]. However, when the bevel angle is lower than 30°, as in our case, the changes in needle deflection as a function of the bevel angle are barely noticeable. Similarly, Jiang *et al* [73] found no significant differences in curvature values for needles with a bevel angle of 30° and 10°. In figures 8(b) and 9 we saw that the needle curvature in the right direction was lower for a larger bevel offset *BO*. This is opposite to our hypothesis. A similar result was also reported in Frasson *et al* [44], who suggested that this unexpected result could have been due to the diameter of the probe, which was larger than regular needles (i.e. 9 mm). A possible explanation of our results could be that the wires tend to bifurcate more for larger *BO* and *S*. If the first pair of advancing wires bifurcates (i.e. first discrete bevel), the second pair of advancing wires may not follow the path laid by the first discrete bevel but lay a new path instead. As a result, the needle would lose the discrete bevel configuration and not deflect towards the desired direction. 3D microscopic observations of bevel-tip needles conducted by Van Veen *et al* [74] showed indeed that the gel rupture at the needle tip is wider and shorter for large bevel angles. A wider and shorter rupture profile provides a larger clearance for the tip to move out of plane. Therefore, it is possible that in the case of a smaller *BO* (i.e. larger bevel angle) the wires had more tendency to move towards the steering direction. The irregular deflection of the wires can also explain the greater variability observed in the results for conditions with large *BO* and *S*.

The value of curvature achieved with this needle design is smaller than the values presented in the state-of-the-art [57, 75]. In future prototypes the resulting steering curvature can be increased in different ways [75]. Designing a needle with a smaller diameter will decrease the bending resistance and therefore increase the curvature [74]; the same result can be obtained by using a material with lower stiffness than Nitinol. It has been also shown that pre-bending a needle can have positive effects on the resulting curvature [26]. It should be noted here that the amount of needle steering needed depends on the medical application. For example, in some cases the steering is used to compensate for tissue or target motion [76–78], and only a small deflection of the needle from the straight path is required (range between 2 mm and 6 mm [77]). The needle presented in this paper can reach deflections up to 7.8 mm (maximum mean value), making it suitable for these types of procedures.

To test whether the needle can change direction of steering without the need of axial rotation, we per-

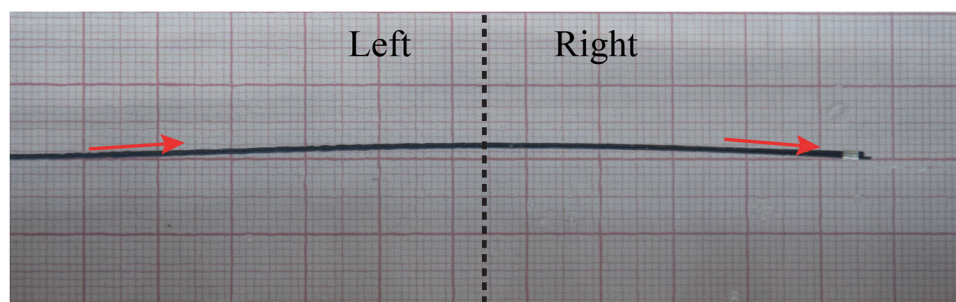


**Figure 10.** Final position of the needle inside the gelatin during the trial in which the steering direction was changed from left to right ( $BO = 0.9$  mm,  $S = 2.0$  mm). Arrows showing the direction of steering and the middle dashed line point when direction changed.

formed three extra trials, in which the wires were actuated clockwise for the first half of the actuation cycles (to steer to the left) and anticlockwise for the second half of the actuation cycles (to steer to the right). These three trials were conducted for  $BO = 0.9$  mm and  $S = 2.0$  mm, which was the combination of  $BO$  and  $S$  that resulted in the least incidences of bifurcation in experiment 2. Besides the limited steering of the needle to the left (see results of experiment 2), a change in direction in the middle of the laid trajectory was noticeable (figure 10).

#### 5.4. Limitations

In experiment 2, higher curvatures were achieved when steering to the right than when steering to the left. This directional preference might have been caused by a tendency of the needle wires to pre-curve. Indeed, after having assembled the needle we observed that the wires at their relaxed state curved slightly to the right.

In our data analysis we assumed that the needle deflection occurs only in the steering plane. However, visual observations showed that the needle also tended to deflect upwards. This upward deflection was not quantified but was present in all our trials and is likely to have been caused by pre-curve in the wires and/or vertical misalignment of the gelatin cart and the actuation unit. Jahya *et al* [79] also reported such ‘out of plane’ deflection and further observed that this deflection increases with the bevel angle of the needle tip. For this reason the absolute values of slip and steering curvature results of experiments 1 and 2 should be interpreted with caution.

In both experiments, the inertia of the gelatin cart and bearing friction might have influenced the slip results. A large mass of gelatin tends to reduce slip in the pushing phase, while the contrary holds during the pulling phase. The friction between the cart which is moving and the base has to be minimal. Parittotokaporn *et al* [53] used a linear air bearing (aerostatic) with a friction coefficient around 0.0001. This value is lower than a typical friction coefficient of a lubricated ball bearing. In our design we opted for ball bearings, because these have a low friction coefficient (0.001–

0.005 [80]) as well as lower costs and maintenance than the air bearings.

#### 5.5. Future work

In future prototypes, we plan to eliminate the pre-curvature in the steering direction by selecting straight annealed Nitinol wires. Different tip designs will be investigated to limit the bifurcation of the wires once they are moved away from the interlocking ring.

A better understanding of the interaction between wires and gelatin could help in explaining the behavior of the needle as a function of  $BO$  and  $S$ . Measurements of friction forces along the needle and forces at the needle tip can be done and used as reference for future design choices, in term of number of wires and actuation method. Furthermore, a stress–strain analyses in the gelatin at the needle tip could give us information on tissue damage during the reciprocal actuation of the wires. Moreover, *ex vivo* experiments are needed for a better understanding of the phenomena in real tissue.

The needle design presented in this paper represents only one of the many possible designs that can originate from our steerable needle concept. The number as well as the diameter of the wires can be changed so that the needle has suitable dimensions for specific applications. A possible application is brachytherapy, where multiple seeds have to be implanted in the prostate; this is usually done with 20–30 needle insertions [81]. Using a needle with enhanced steerability, it would be possible to use only one needle and change the direction of the needle ‘on-the-spot’ without the need of multiple punctures, reducing pain and tissue damage.

## 6. Conclusion

This paper presents the design and experimental evaluation of a wasp ovipositor-inspired needle with a diameter of 1.2 mm. We showed that the needle can penetrate a gelatin phantom of 4 wt% with zero external push force, and that it steers by means of a ‘discrete’ bevel-tip. The proposed biologically inspired needle design is an important step towards

the development of ultra-thin steerable needles for percutaneous interventions.

## Acknowledgments

This research is supported by the the Netherlands Organization for Scientific Research (NWO), domain Applied and Engineering Sciences (TTW), and which is partly funded by the Ministry of Economic Affairs (project number 12712, STW Perspectief Programme iMIT-Instruments for Minimally Invasive Techniques). The authors would like to thank Menno Lageweg and Danny de Gans from the Central Workshop (DEMO) of the TU Delft for their design advice and needle prototype manufacturing.

## ORCID iDs

M Scali  <https://orcid.org/0000-0002-9272-473X>

D Dodou  <https://orcid.org/0000-0002-9428-3261>

## References

- Phelan S, O'Doherty A, Hill A and Quinn C M 2006 Epithelial displacement during breast needle core biopsy causes diagnostic difficulties in subsequent surgical excision specimens *J. Clin. Pathol.* **60** 373–6
- Volpe A, Kachura J R, Geddie W R, Evans A J, Gharajeh A, Saravanan A and Jewett M A 2007 Techniques, safety and accuracy of sampling of renal tumors by fine needle aspiration and core biopsy *J. Urol.* **178** 379–86
- Podder T K, Dicker A P, Hutapea P, Darvish K and Yu Y 2012 A novel curvilinear approach for prostate seed implantation *Med. Phys.* **30** 1887–92
- Wan G, Wei Z, Gardi L, Downey D B and Fenster A 2005 Brachytherapy needle deflection evaluation and correction *Med. Phys.* **32** 902–9
- Jeng C L, Torrillo T M and Rosenblatt M A 2010 Complications of peripheral nerve blocks *Br. J. Anaesth.* **105** 97–107
- Maddali P, Moisi M, Page J, Chamiraju P, Fisahn C, Oskouian R and Tubbs R S 2017 Anatomical complications of epidural anesthesia: a comprehensive review *Clin. Anat.* **30** 342–6
- Kohn L T, Corrigan J M and Donaldson M S 2000 *To Err is Human: Building a Safer Health System* (Washington, DC: National Academy of Science) (<https://doi.org/10.17226/9728>)
- Palisch A, Patel R G, Gutowski C, Zoga A C, Colucci P, O'Hara B J, Roberts C C and Abraham J 2016 Analysis of needle type for musculoskeletal lesion biopsy: results of a novel steerable needle *Curr. Orthop. Pract.* **27** 393–9
- Scali M, Pusch T P, Breedveld P and Dodou D 2016 Needle-like instrument for steering through solid organs: a review of the scientific and patent literature *Proc. Inst. Mech. Eng. H* **231** 250–65
- Swaney P J, Burgner J, Gilbert H B and Webster R J 2013 A flexure-based steerable needle: High curvature with reduced tissue damage *IEEE Trans. Biomed. Eng.* **60** 906–9
- Drummond G B and Scott D H 1980 Deflection of spinal needles by the bevel *Anaesthesia* **35** 854–7
- Wang Y Z, Yin Q L, Liu C J and Chen Y H 2012 Towards an articulated needle *Appl. Mech. Mater.* **152** 946–51
- Kuhle W G 1999 Biopsy needle with flared tip *US Patent* 5938635
- Okazawa S, Ebrahimi R, Chuang J, Salcudean S E and Rohling R 2005 Hand-held steerable needle device *IEEE/ASME Trans. Mechatronics* **10** 285–96
- Torabi M, Gupta R and Walsh C J 2014 Compact robotically steerable image guided instrument for multi-adjacent-point (MAP) targeting *IEEE Trans. Robot.* **30** 802–15
- Misra S, Reed K B, Douglas A S, Ramesh K T and Okamura A M 2008 Needle-tissue interaction forces for bevel-tip steerable needles *2nd IEEE RAS EMBS Int. Conf. on Biomedical Robotics and Biomechanics* pp 224–31
- Webster R J, Kim J S, Cowan N J, Chirikjian G S and Okamura A M 2006 Nonholonomic modeling of needle steering *Int. J. Robotics Res.* **25** 509–25
- Minhas D S, Engh J A, Fenske M M and Riviere C N 2007 Modeling of needle steering via duty cycled spinning *29th Annual Int. Conf. of the IEEE Engineering in Medicine and Biology Society* pp 2756–9
- Kraft D and Hole J 2008 Device and method for rapid aspiration and collection of body tissue from within an enclosed body space *US Patent* 9131925
- Pellegrino R, Patel S and Carrison H 2013 Systems and methods for navigating an instrument through bone *WO Patent* 2011085212
- Kaplan E J 2007 Deflectable implantation device and method of use *US Patent* 7282020
- Webster R J, Okamura A M and Cowan N J 2006 Toward active cannulas: miniature snake-like surgical robots *IEEE/RSJ Int. Conf. on Intelligent Robots and Systems (IROS)* pp 2857–63
- Bui V K, Park S, Park J O and Ko S Y 2016 A novel curvature-controllable steerable needle for percutaneous intervention *Proc. Inst. Mech. Eng. H* **230** 727–38
- van de Berg N J, Dankelman J and van den Dobbelsteen J J 2015 Design of an actively controlled steerable needle with tendon actuation and FBG-based shape sensing *Med. Eng. Phys.* **37** 617–22
- Losey D P, York P A, Swaney P J, Burgner J and Webster R J III 2013 A flexure-based wrist for needle-sized surgical robots *Proc. SPIE 8671, Medical Imaging: Image-Guided Procedures, Robotic Interventions, and Modeling* **8671**
- Adebar T K, Greer J D, Laeseke P F, Hwang G L and Okamura A M 2016 Methods for improving the curvature of steerable needles in biological tissue *IEEE Trans. Biomed. Eng.* **63** 1167–77
- Ayvali E, Ho M and Desai J P 2014 A novel discretely actuated steerable probe for percutaneous procedures *Exp. Robot. ed O Khatib et al Springer Tracts in Advanced Robotics* vol 79 (Berlin: Springer) pp 115–23
- Konh B, Lee H, Lee H H, Zhao V, Martin V P and Hutapea P 2015 Towards the design and development of an active needle for therapeutic procedures *41st IEEE Annual Northeast Biomedical Engineering Conf.* pp 1–2
- Yan K, Podder T, Ng W S and Yu Y 2007 Smart needle for percutaneous surgery: Influential factor investigation *29th Annual Int. Conf. of the IEEE Engineering in Medicine and Biology Society* pp 461–4
- Swensen J P, Lin M, Okamura A M and Cowan N J 2014 Torsional dynamics of steerable needles: modeling and fluoroscopic guidance *IEEE Trans. Biomed. Eng.* **61** 2707–17
- Reed K B, Okamura A M and Cowan N J 2009 Modeling and control of needles with torsional friction *IEEE Trans. Biomed. Eng.* **56** 2905–16
- Reed K B, Majewicz A, Kallem V, Alterovitz R, Goldberg K, Cowan N J and Okamura A M 2011 Robot-assisted needle steering *IEEE Robot. Autom. Mag.* **18** 35–46
- Le Lannic J and Nénon J P 1999 Functional morphology of the ovipositor in *Megarhyssa atrata* (Hymenoptera, Ichneumonidae) and its penetration into wood *Zoomorphology* **119** 73–9
- Kundanati L and Gundiah N 2014 Biomechanics of substrate boring by fig wasps *J. Exp. Biol.* **217** 1946–54
- Vincent J F and King M J 1995 The mechanism of drilling by wood wasp ovipositors *Biomimetics* **3** 187–201

- [36] Rahman M H, Fitton M G and Quicke D L 1998 Ovipositor internal microsculpture in the Braconidae (Insecta, Hymenoptera) *Zool. Scr.* **27** 319–32
- [37] Quicke D L, Wyeth P, Fawke J D, Basibuyuk H H and Vincent J F 1998 Manganese and zinc in the ovipositors and mandibles of hymenopterous insects *Zool. J. Linnean Soc.* **24** 387–96
- [38] Quicke D L, Fitton M G and Harris J 1995 Ovipositor steering mechanisms in braconid wasps *J. Hymenopt. Res.* **4** 110–20
- [39] Quicke D L and Fitton M G 1995 Ovipositor steering mechanisms in parasitic wasps of the families Gasteruptiidae and Aulacidae (Hymenoptera) *Proc. R. Soc. B* **261** 99–103
- [40] Pollard D 1969 Directional control of the stylets in phytophagous Hemiptera *Physiol. Entomol.* **44** 173–85
- [41] Gao Y, Ellery A, Jaddou M and Vincent J 2006 Deployable wood wasp drill for planetary subsurface sampling *IEEE Aerospace Conf.* p 8
- [42] Frasson L, Ko S Y, Turner A, Parittotokkaporn T, Vincent J F and Rodriguez y Baena F 2010 STING: a soft-tissue intervention and neurosurgical guide to access deep brain lesions through curved trajectories *Proc. Inst. Mech. Eng. H* **224** 775–88
- [43] Ko S Y, Davies B L and Rodriguez y Baena F 2010 Two-dimensional needle steering with a ‘programmable bevel’ inspired by nature: modeling preliminaries *IEEE Int. Conf. on Intelligent Robots* pp 2319–24
- [44] Frasson L, Ferroni F, Ko S Y, Dogangil G and Rodriguez y Baena F 2012 Experimental evaluation of a novel steerable probe with a programmable bevel tip inspired by nature *J. Robot. Surg.* **6** 189–97
- [45] Frasson L, Reina S, Davies B L and Rodriguez y Baena F 2009 Design optimisation of a biologically inspired multi-part probe for soft tissue surgery *World Congress on Medical Physics and Biomedical Engineering (Munich)* ed O Dössel and W C Schlegel *IFMBE Proceedings* vol 25 (Berlin: Springer) pp 307–10
- [46] Frasson L, Neubert J, Reina S, Oldfield M, Davies B L and Rodriguez y Baena F 2010 Development and validation of a numerical model for cross-section optimization of a multi-part probe for soft tissue intervention *Annual Int. Conf. of the IEEE Engineering in Medicine and Biology Society* pp 3202–5
- [47] Leibinger A, Oldfield M and Rodriguez y Baena F 2014 Multi-objective design optimization for a steerable needle for soft tissue surgery *15th Int. Conf. on Biomedical Engineering* ed J Goh *IFMBE Proceedings* vol 43 (Cham: Springer) pp 420–3
- [48] Frasson L, Parittotokkaporn T, Schneider A, Davies B L, Vincent J F V, Hup S E, Degenaar P and Rodriguez y Baena F 2008 Biologically inspired microtexturing: investigation into the surface topography of next-generation neurosurgical probes *30th Int. Conf. of the IEEE Engineering in Medicine and Biology Society* pp 5611–4
- [49] Schneider A, Frasson L, Parittotokkaporn T, Rodriguez y Baena F, Davies B L and Huq S E 2009 Biomimetic microtexturing for neurosurgical probe surfaces to influence tribological characteristics during tissue penetration *Microelectron. Eng.* **86** 1515–7
- [50] Schneider A, Frasson L, Parittotokkaporn T, Rodriguez y Baena F, Davies B L and Huq S 2008 Microfabrication of components for a novel biomimetic neurological endoscope *4th Int. Conf. on Multi-Material Micro Manufacture* pp 9–11
- [51] Parittotokkaporn T, Thomas D G T, Huq E, Davies B L, Degenaar P and Rodriguez y Baena F 2012 Microtextured surfaces for deep-brain stimulation electrodes: a biologically inspired design to reduce lead migration *World Neurosurg.* **77** 569–76
- [52] Frasson L, Parittotokkaporn T, Davies B L and Rodriguez y Baena F 2009 Early developments of a novel smart actuator inspired by nature *Int. J. Intell. Syst. Technol. Appl.* **8** 409–22
- [53] Parittotokkaporn T, Frasson L, Schneider A, Huq S E, Davies B L, Degenaar P, Biesenack J and Rodriguez y Baena F 2008 Soft tissue traversal with zero net force: feasibility study of a biologically inspired design based on reciprocal motion *IEEE Int. Conf. on Robotics and Biomimetics* pp 80–5
- [54] Parittotokkaporn T, Frasson L, Schneider A, Davies B L, Degenaar P and Rodriguez y Baena F 2010 Insertion experiments of a biologically inspired microtextured and multi-part probe based on reciprocal motion *Annual Int. Conf. of the IEEE Engineering in Medicine and Biology Society* pp 3190–3
- [55] Oldfield M, Dini D, Giordano G and Rodriguez y Baena F 2013 Detailed finite element modelling of deep needle insertions into a soft tissue phantom using a cohesive approach *Comput. Methods Biomech. Biomed. Eng.* **16** 530–43
- [56] Secoli R and Rodriguez y Baena F 2013 Closed-loop 3D motion modeling and control of a steerable needle for soft tissue surgery *IEEE Int. Conf. on Robotics and Automation* pp 5831–6
- [57] Ko S Y, Frasson L and Rodriguez y Baena F 2011 Closed-loop planar motion control of a steerable probe with a ‘programmable bevel’ inspired by nature *IEEE Trans. Robot.* **27** 970–83
- [58] Burrows C, Secoli R and Rodriguez y Baena F 2013 Experimental characterisation of a biologically inspired 3D steering needle *13th Int. Conf. on Control, Automation and Systems* pp 1252–7
- [59] Burrows C, Liu F, Leibinger A, Secoli R and Rodriguez y Baena F 2017 Multi-target planar needle steering with a bio-inspired needle design *Advances in Italian Mechanism Science* ed Boschetti G and Gasparetto A *Mechanisms and Machine Science* vol 47 (Cham: Springer) pp 51–60
- [60] Leibinger A, Oldfield M J and Rodriguez y Baena F 2016 Minimally disruptive needle insertion: a biologically inspired solution *Interface Focus* **6** 20150107
- [61] Sprang T, Breedveld P and Dodou D 2016 Wasp-inspired needle insertion with low net push force *Biomimetic and Biohybrid Systems Living Machines* ed N Lepora et al *Lecture Notes in Computer Science* vol 9793 (Cham: Springer) pp 307–18
- [62] Gherardi G 2009 *Fine-Needle Biopsy of Superficial and Deep Masses: Interventional Approach and Interpretation Methodology by Pattern Recognition* (Verlag: Springer) (<https://doi.org/10.1007/978-88-470-1433-6>)
- [63] Podder T et al 2006 *In vivo* motion and force measurement of surgical needle intervention during prostate brachytherapy *Med. Phys.* **33** 2915–22
- [64] Scali M, Pusch T P, Breedveld P and Dodou D 2016 Design and preliminary evaluation of a bio-inspired steerable needle *28th Int. Conf. Society for Medical Innovation and Technology*
- [65] Rogers D 1972 The ichneumon wasp *Venturia canescens*: oviposition and avoidance of superparasitism *Entomol. Exp. Appl.* **15** 190–4
- [66] Chatelin S, Constantinesco A and Willinger R 2010 Fifty years of brain tissue mechanical testing: from *in vitro* to *in vivo* investigations *Biorheology* **47** 255–76
- [67] Webster R J, Memisevic J and Okamura A M 2005 Design considerations for robotic needle steering *IEEE Int. Conf. on Robotics and Automation* pp 3588–94
- [68] Misra S, Reed K B, Schafer B W, Ramesh K T and Okamura A M 2010 Mechanics of flexible needles robotically steered through soft tissue *Int. J. Robot. Res.* **29** 1640–60
- [69] Konh B, Honarvar M, Darvish K and Hutapea P 2016 Simulation and experimental studies in needle–tissue interactions *J. Clin. Monit. Comput.* **31** 1–12
- [70] Swensen J P and Cowan N J 2012 Torsional dynamics compensation enhances robotic control of tip-steerable needles *IEEE Int. Conf. on Robotics and Automation* pp 1601–6
- [71] van Gerwen D J, Dankelman J and van den Dobbelsteen J J 2012 Needle–tissue interaction forces—A survey of experimental data *Med. Eng. Phys.* **34** 665–80
- [72] Hing J T, Brooks A D and Desai J P 2006 Reality-based needle insertion simulation for haptic feedback in prostate brachytherapy *IEEE Int. Conf. on Robotics and Automation* pp 619–24

- [73] Jiang S and Wang X 2016 Mechanics-based interactive modeling for medical flexible needle insertion in consideration of nonlinear factors *J. Comput. Nonlin. Dyn.* **11** 011004
- [74] van Veen Y R, Jahya A and Misra S 2012 Macroscopic and microscopic observations of needle insertion into gels *Proc. Inst. Mech. Eng. H* **226** 441–9
- [75] Scali M, Kreeft D, Breedveld P and Dodou D 2017 Design and evaluation of a wasp-inspired steerable needle *Proc. SPIE 10162, Bioinspiration, Biomimetics, and Bioreplication* pp 1016207–13
- [76] Abolhassani N, Patel R V and Ayazi F 2007 Minimization of needle deflection in robot-assisted percutaneous therapy *Int. J. Med. Robot.* **3** 140–8
- [77] Stone N N, Roy J, Hong S, Lo Y C and Stock R G 2002 Prostate gland motion and deformation caused by needle placement during brachytherapy *Brachytherapy* **1** 154–60
- [78] Sadjadi H, Hastrudi Z K and Fichtinger G 2014 Needle deflection estimation: prostate brachytherapy phantom experiments *Int. J. Comput. Assist. Radiol. Surg.* **9** 921–9
- [79] Jahya A, van der Heijden F and Misra S 2012 Observations of three-dimensional needle deflection during insertion into soft tissue *4th IEEE RAS EMBS Int. Conf. on Biomedical Robotics and Biomechatronics* pp 1205–10
- [80] Powell J W 1970 *Design of Aerostatic Bearings* (Brighton: Machinery Publishing)
- [81] Alterovitz R, Pouliot J, Taschereau R, Hsu I C and Goldberg K 2003 Simulating needle insertion and radioactive seed implantation for prostate brachytherapy *Studies in Health Technology and Informatics* ed J D Westwood et al *Medicine Meets Virtual Reality 11* vol 94 (Amsterdam: IOS Press) 19–25